Tectonophysics 746 (2018) 587–601

Contents lists available at ScienceDirect

Tectonophysics

journal homepage: www.elsevier.com/locate/tecto

What drives metamorphism in early Archean greenstone belts? Insights from numerical modeling

Elena Sizova [a,*], Taras Gerya [b,c], Michael Brown [d], Kurt Stüwe [a]

[a] Department of Earth Science, Karl-Franz University of Graz, Austria
[b] ETH-Zurich, Institute of Geophysics, Switzerland
[c] Adjunct Professor of Geology Department, Moscow State University, Moscow 119199, Russia
[d] Department of Geology, University of Maryland, College Park, MD 20742, USA

ARTICLE INFO

Article history:
Received 1 June 2017
Received in revised form 7 July 2017
Accepted 23 July 2017
Available online 25 July 2017

Keywords:
Archean
Dome-and-keel structure
Granite–greenstone belts
Metamorphism
P–T–t paths
Vertical and horizontal tectonics

ABSTRACT

Geodynamic regimes responsible for the formation of Eoarchean-to-Mesoarchean continental crust may be investigated using numerical modeling in which deeper mantle processes are coupled with shallower processes responsible for the formation and modification of the crust. In an earlier study using a 2D coupled petrological–thermomechanical tectono-magmatic numerical model constrained by information from the geological record, experiments with initial conditions appropriate to the Eoarchean–Mesoarchean revealed multiple tectonic processes by which mostly felsic continental crust could have been formed from an initial primary mafic crust in a non-uniformitarian geodynamic regime. We use the model pressure–temperature–time (*P–T–t*) paths for material particles from our previous study to test the hypothesis that the range of metamorphic *P–T* conditions recorded in Archean granite–greenstone domains could have been generated without subduction and plate tectonics. We compare the experimental results with *P–T* and age data recovered from two early Archean domains, the East Pilbara Terrane (EPT), part of the Pilbara craton in Western Australia, and the Barberton greenstone belt (BGB), part of the Kapvaal craton in South Africa. The dome-and-keel structures that develop in the crust in the numerical experiment and the associated *P–T–t* paths at various locations within these structures are similar to the structures and *P–T* and age data recovered from the early Archean crust in the EPT and BGB. This study shows that metamorphism in granite–greenstone-like crust could have been the result of both vertical and horizontal tectonic processes (coupled with crustal convective overturns) that occurred over linked sites of crustal delamination and mantle upwelling. The range of thermal gradients derived from peak *P–T* values for markers in the experiment matches the range of apparent thermal gradients retrieved from the EPT and BGB, demonstrating that even the lowest apparent thermal gradients associated with dome-and-keel structures in greenstone belts can be achieved in the absence of subduction.

1. Introduction

It is thought that mantle potential temperatures were higher in the Archean, although how much higher than the present day and whether the mantle was warming during the Eoarchean–Mesoarchean to a high in the Mesoarchean–Neoarchean are both open questions (Herzberg et al., 2007, 2010). The limited preservation of Eoarchean–Mesoarchean crust combined with the poorly-constrained thermal evolution of Earth prior to 3.0 Ga (Korenaga, 2013; Labrosse and Jaupart, 2007; Silver and Behn, 2008; Van Hunen and Moyen, 2012) has led to uncertainty regarding the dominant geodynamic regime during the Archean (Benn et al., 2006; Gerya, 2014 and references therein).

Exposed crust of Archean age is dominated by the tonalite–trondhjemite–granodiorite (TTG) suite of rocks. Within Archean cratons two distinct types of crustal domain have been recognized: lower metamorphic grade granite (TTG)–greenstone belts with dome-and-keel structure, and higher metamorphic grade grey gneiss complexes dominated by TTGs but with greenstone relicts. In an early interpretation, Windley and Bridgwater (1971) proposed that these two domains corresponded to the upper- and lower-parts of the Archean crust. Recently Johnson et al. (2016) argued that the high-grade Lewisian Complex, part of the North Atlantic craton, is an example of Archean lower crust formed beneath a granite–greenstone domain in the upper crust. By contrast, Van Kranendonk (2010) proposed that the two different types of crust formed in different tectonic settings, one over upwelling mantle (granite–greenstone belts) and the other associated with subduction (high-grade gneiss complexes).

* Corresponding author.
E-mail address: elena.sizova@uni-graz.at (E. Sizova).

http://dx.doi.org/10.1016/j.tecto.2017.07.020
0040-1951/

Given the higher mantle potential temperature and the uncertainty over the dominant geodynamic regime in the Archean, numerical modeling provides an important method by which to gain insight into the evolution of Earth in the Archean (Fischer and Gerya, 2016a, 2016b; Johnson et al., 2014; Sizova et al., 2010, 2015). To do this, global and regional-scale thermo-mechanical numerical models that have been validated for present day conditions on Earth are extrapolated back in time to test the contrasting ideas discussed above (Sizova et al., 2010). Recently, Sizova et al. (2015) used a 2D numerical model with parameters appropriate to the Archean to investigate the formation of early Archean TTG crust. The model includes spontaneous plate generation and movement, partial melting, melt extraction and melt emplacement resulting in crustal growth, radiogenic heat production and eclogitization. The results reported by Sizova et al. (2015) demonstrated several possible tectonic settings for the formation of TTGs and identified the sequential development of two different types of crust, namely granite–greenstone-like crust with dome-and-keel geometry, and reworked (accreted) crust comprising strongly deformed granite–greenstone domains and subduction-related sequences. Here we test the relevance of these predictions to the evolution of the Archean crust through a careful comparison of pressure (P)–temperature (T)–time (t) paths for material particles (markers) in the experiment with P–T paths and age data retrieved from natural Archean terrains observed in the field.

Two of the most thoroughly studied examples of early Archean granite–greenstone domains are the East Pilbara Terrane of the Pilbara Craton in Western Australia and the Barberton granite–greenstone belt in South Africa. The geodynamic setting proposed for both of these domains is controversial: either sagduction and partial convective overturn associated with upwelling mantle (e.g. Brown, 2015; François et al., 2014; Hickman, 2004; Sizova et al., 2015; Thébaud and Rey, 2013; Van Kranendonk, 2010, 2011; Van Kranendonk et al., 2007, 2009, 2014, 2014; Wiemer et al., 2016), or related to a convergent plate margin (e.g. Blewett, 2002; Blewett et al., 2004; Cutts et al., 2014; de Ronde and Kamo, 2000; Diener et al., 2005, 2006; Kisters et al., 2003, 2010; Kloppenburg et al., 2001; Moyen et al., 2006). Although there is much accumulated field evidence and structural data from both examples (*op. cit.*), these data have not been sufficient to discriminate one model from the other. For example, two detailed studies of the polyphase structural evolution of greenstones, one on the southwest side of the Mount Edgar granitoid dome (Warrawoona greenstone belt; Kloppenburg et al., 2001) and the other on the northwestern side (the Doolena greenstone belt; Wiemer et al., 2016), arrive at different conclusions, supporting plate tectonic processes in the first case and sagduction associated with partial convective overturn in the second. The same dichotomy occurs at Barberton, where integrated field and laboratory studies have been interpreted to support convergence with a west- or northwest-directed subduction polarity (Diener et al., 2005; Kisters et al., 2010; Moyen et al., 2006) or partial convective overturn in a non-uniformitarian geodynamic regime (Brown, 2015; Van Kranendonk et al., 2009, 2014). In the southwestern sector of the Barberton granite–greenstone belt, apparent thermal gradients for the peak pressure metamorphic conditions have been estimated to lie in the range 70–50 °C/kbar (Moyen et al., 2006). Although these thermal gradients are not as low as those generated by subduction at the present day (Syracuse et al., 2010), they have been used to support the plate margin hypothesis for the evolution of the Barberton granite–greenstone belt.

Numerical modeling permits exploration of the relationship between the P–T–t evolution of particular markers in the model crust and the tectonic setting within a prescribed geodynamic regime, which may then be compared with natural data. In this study, we plot the P–T–t paths of markers located in greenstones in the granite–greenstone-like crust from the reference experiment of Sizova et al. (2015) and compare these to data retrieved from the two natural examples of Paleoarchean–Mesoarchean granite–greenstone domains discussed above. Our objective is to test the null hypothesis that the metamorphic P–T conditions recorded in the natural greenstone belts are incompatible with sagduction and crustal diapirism associated with upwelling mantle. Our study complements the regional study and numerical modeling of François et al. (2014) for the East Pilbara Terrane. Our results show the metamorphic P–T conditions recorded in the exemplar greenstone belts are generally compatible with those retrieved from the numerical model, contrary to the null hypothesis, leading us to conclude that apparent thermal gradients and peak metamorphic conditions in early Archean greenstones may not be uniquely diagnostic of a convergent plate margin.

2. Examples of early Archean granite–greenstone domains

2.1. The East Pilbara Terrane

The East Pilbara Terrane (EPT) is characterized by multiphase granitoid domes, mostly composed of rocks of the tonalite–trondhjemite–granodiorite (TTG) suite, and intervening greenstone belts comprising predominantly low-grade metamorphosed ultramafic–mafic volcanic and sedimentary rocks (Fig. 1). A widely accepted interpretation of the dome-and-keel structure of the EPT is that it formed by intermittent episodes of doming driven by partial convective overturn of the thick, dense greenstone succession into a partially molten granitic middle crust in the interval 3.53 to 3.24 Ga (e.g., Collins et al., 1998; Collins and Van Kranendonk, 1999; François et al., 2014; Hickman, 1984, 2004; Hickman and Van Kranendonk, 2004; Van Kranendonk et al., 2004, 2007; Wiemer et al., 2016; Johnson et al., 2017; Gardiner et al., 2017). In a contrasting interpretation, others have argued that the structures record episodes of orthogonal extension and shortening (Blewett, 2002) or require convergent plate margin processes rather than diapirism (Kloppenburg et al., 2001).

In general, the greenstones away from the TTG domes are relatively undeformed and mainly characterized by a very low-pressure prehnite–pumpellyite to greenschist facies metamorphic overprint, as for example in the North Pole area (Fig. 1, Kitajima et al., 2001; Terabayashi et al., 2003). However, near the margins of the TTG domes the strain is higher and the metamorphic grade reaches amphibolite facies (Collins and Van Kranendonk, 1999; Delor et al., 1991; François et al., 2014). For example, to the west of the Corruna Downs granitoid dome (Fig. 1) the higher-grade supracrustal rocks include metapelites in which kyanite has been partially replaced by sillimanite; conventional thermobarometry on these rocks yields P of 6 ± 1 kbar at T of ~450 to

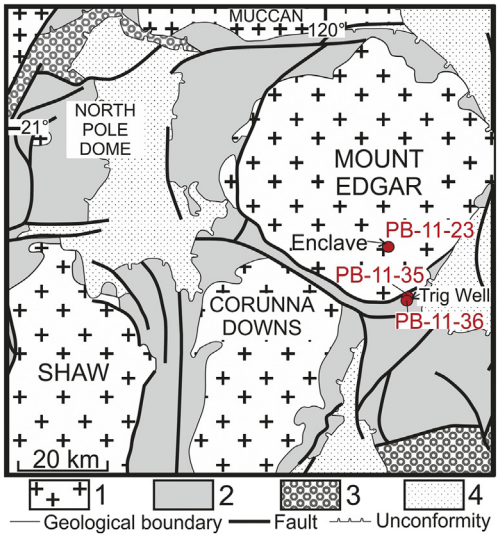

Fig. 1. A simplified geological map of the East Pilbara Terrane (modified from Blewett et al., 2004) with the location of samples discussed in the text and used for comparison with results from the experiment in Fig. 11 below. 1 = Granitoid rocks; 2 = Pilbara Supergroup rocks; 3 = De Grey Supergroup rocks; and, 4 = Fortescue Supergroup rocks.

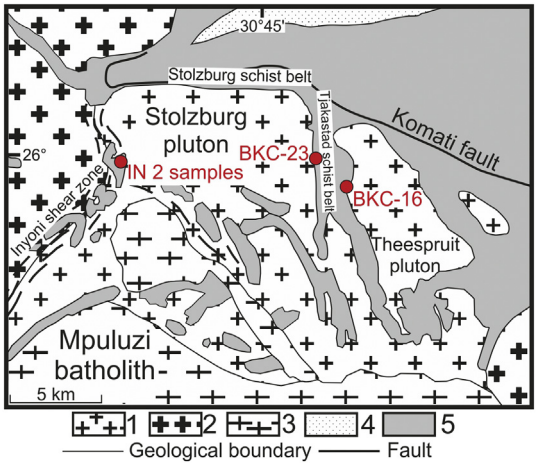

Fig. 2. A simplified geological map of the Barberton granite–greenstone belt (modified from Diener et al., 2006) with the location of samples discussed in the text and used for comparison with results from the experiment in Fig. 11 below. 1 = ca 3.45 TTG plutons; 2 = ca 3.23 TTG plutons; 3 = ca 3.1 Ga potassic granite; 4 = Moodies Group; and, 5 = Onverwacht Group.

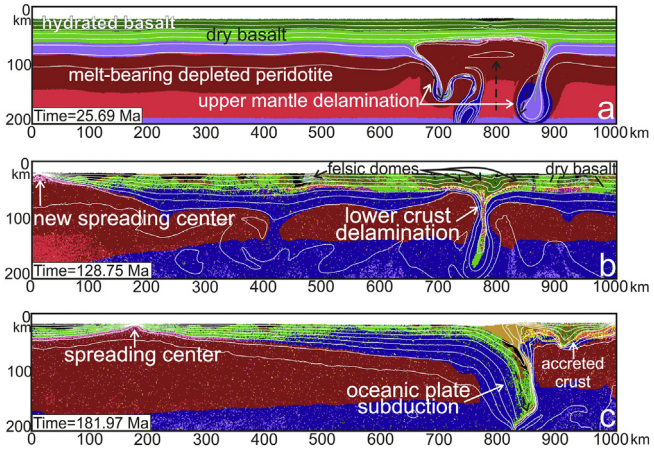

Fig. 4. Representative time-slice snapshots to show the main stages of the evolution of the reference experiment from Sizova et al. (2015): (a) simultaneous upwelling of the asthenospheric mantle and delamination of the mantle lithosphere and part of the lower portion of the overlying mafic crust; (b) mantle upwelling at the left-hand boundary causing shortening of the continent-like crust with felsic domes at the right-hand side; (c) subduction of the newly produced ocean plate from the left under the reworked continent-like crust at the right-hand side.

~600 °C (Delor et al., 1991). In the Warrawoona greenstone belt, which is located between the northern margin of the Corruna Downs granitoid dome and the southern margin of the Mount Edgar granitoid dome (Fig. 1), maximum metamorphic pressures are higher and the rocks appear to record *P–T* paths dominated by decompression. At the eastern end of the greenstone belt, at Trig Well, two samples (Fig. 1; PB-11-35 and -36) define overlapping phase assemblage fields on *P–T* pseudosections that yield *P* decreasing from ~9 to <5 kbar at *T* of 600 ± 20 °C (François et al., 2014). Collins and Van Kranendonk (1999) suggested that such rocks may represent the deeper-level marginal supracrustal rocks exhumed and juxtaposed against their lower-grade equivalents during later doming events. To the north of Trig Well within the Mount Edgar granitoid, the peak phase assemblage field on a *P–T* pseudosection for a metasedimentary enclave (Fig. 1; sample PB-11-23) yields *P–T* conditions of 5.5 ± 1.5 kbar at 690 ± 35 °C (François et al., 2014).

François et al. (2014) report two ages of metamorphism. An older monazite age of *c.* 3.443 Ga was retrieved from lower amphibolite facies garnet–staurolite–andalusite schist from south of the Chinaman shear zone towards the southwest margin of the Mount Edgar dome. By contrast, zircon from an enclave of garnet-bearing migmatite within the Mount Edgar dome to the east yielded a zircon age of *c.* 3.312 Ga. These two ages correspond to the older gneissic (3.47–3.43 Ga) and younger granodiorite (3.32–3.29 Ga) components of the Mount Edgar dome (Kloppenburg, 2003; Williams and Collins, 1990). Collins et al. (1998) argued that partial melting of sialic crust occurred during crustal overturn and proposed such thermal softening to be a necessary condition for triggering partial convective overturn. The heat to generate the necessary partial melting in the EPT could have been derived from conductive cooling of the mantle plume considered to have been responsible

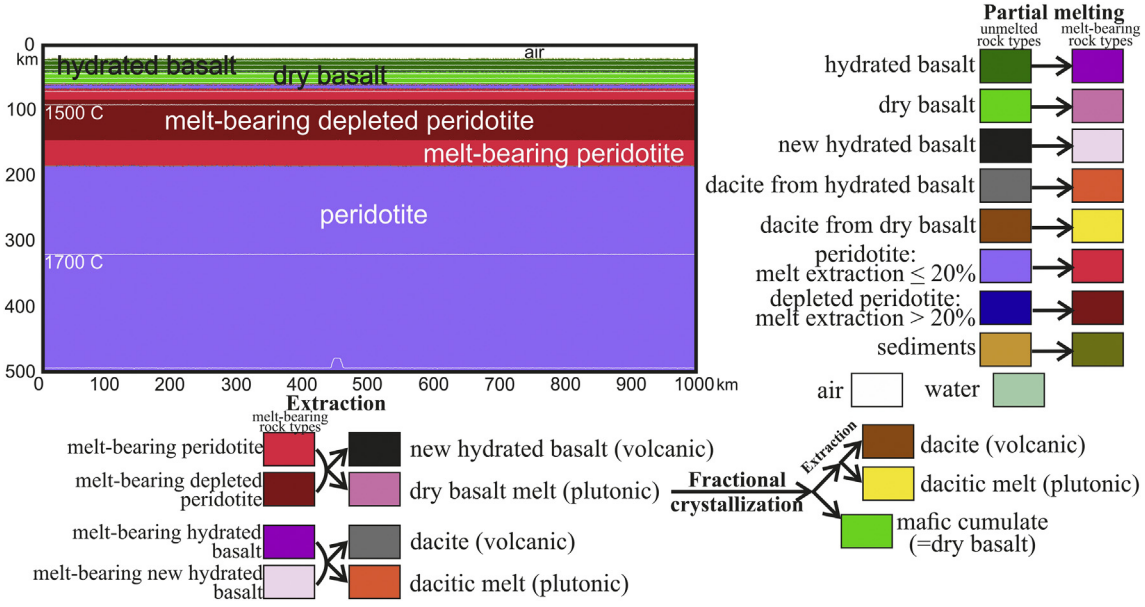

Fig. 3. Initial configuration of the experiment (from Sizova et al., 2015). White lines are isotherms shown for increments of 200 °C starting from 100 °C. Colors indicate materials (e.g. rock type or melt) which appear in subsequent figures. The interrelations between the materials used in the experiment including, partial melting and melt extraction, are shown with arrows. The resolution of the model is 2 × 2 km. Note that the top of the crust in the model and in the subsequent figures is located at 20 km depth due to the layer of air/water above the crust, which is a necessary component of the numerical model.

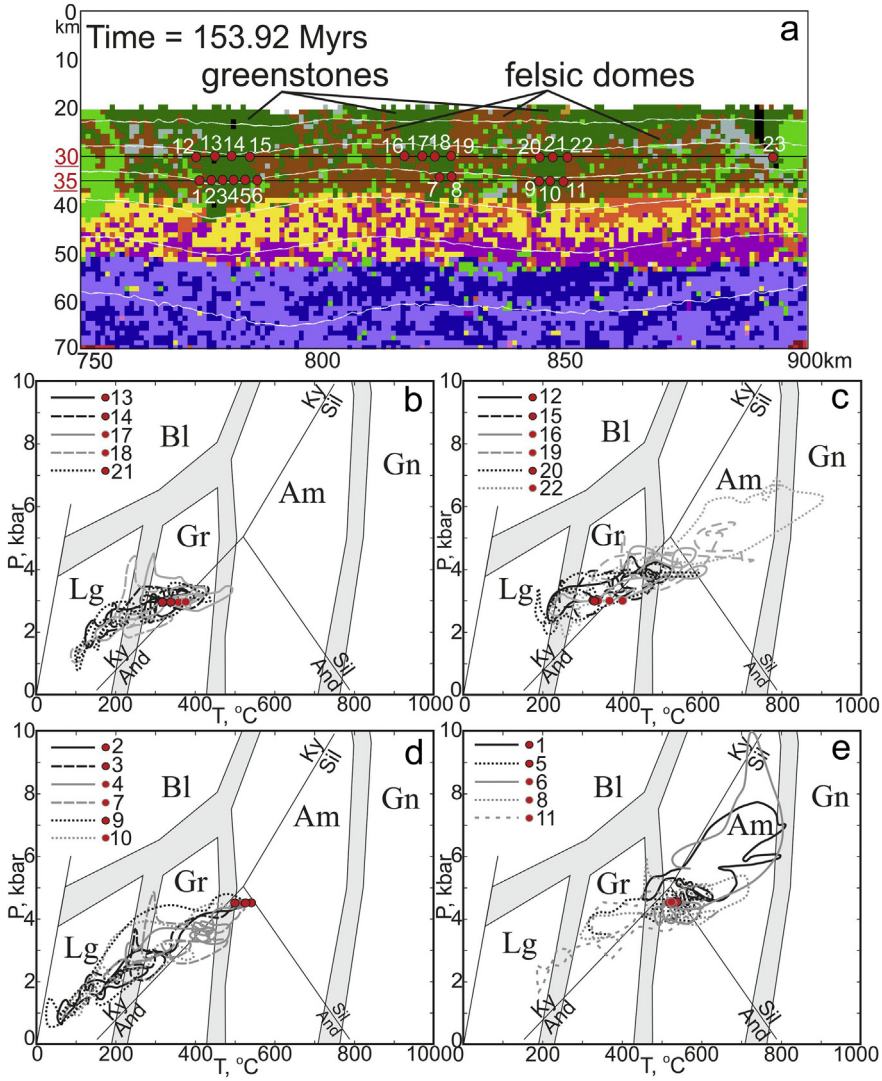

Fig. 5. A representative snapshot from the experiment (150 × 70 km section of the original 1000 × 500 km model) at 153.92 Myrs to show the granite–greenstone-like crust with dome-and-keel geometry (a). Numbered red circles on the snapshot (a) are markers that refer to the diagrams with the *P–T–t* paths (b–e) shown from the start of the experiment up to the time of the snapshot (a). (b) *P–T–t* paths for markers at 10 km below the top of the crust (30 km depth in the model) located in the interior of the greenstone keels. (c) *P–T–t* paths for markers at 10 km below the top of the crust (30 km depth in the model) in greenstones close to the dome margins. (d) *P–T–t* paths for markers at 15 km below the top of the crust (35 km depth in the model) located in the interior of the greenstone keels. (e) *P–T–t* paths for markers at 15 km below the top of the crust (35 km depth in the model) in greenstones close to the dome margins. Metamorphic facies fields (separated by grey fields) on these and all following *P–T* diagrams are modified from Fig. 1 in Brown (2014): Lg = low-grade metamorphism, Bl = blueschist facies, Gr = greenschist facies, Am = Amphibolite facies, Gn = granulite facies. Errors associated with the *P–T* values retrieved from the experiment are ±5 °C and ±0.1 kbar.

for the komatiite-bearing Upper Warrawoona group (Collins et al., 1998).

2.2. The Barberton granite–greenstone belt

Although the Barberton granite–greenstone belt (BGB) in South Africa is characterized by dome-and-keel architecture (Kisters and Anhaeusser, 1995; Fig. 1), similar to that in the EPT, the interpretation of its origin is even more controversial. The main points of contention are: (1) whether the Saddleback–Inyoka fault system and its extension to the Inyoni shear zone to the southwest, which separates a northern from a southern terrane in the BGB (Fig. 1), represents an arc–arc collision at a convergent plate boundary, as proposed by de Ronde and de Wit (1994); and, (2) within the southern terrane, whether the juxtaposition of lower-grade greenstones to the north of the Komati fault in the interior of the belt against the higher-grade tonalite–trondhjemite–granodiorite gneisses and amphibolites to the south of the Komati fault (Fig. 1) was a consequence of gravitational collapse of crust thickened by convergent plate margin processes forming a core complex, as proposed by Kisters et al. (2003). The putative arc collision occurred in the interval ca. 3.29–3.26 Ga (de Ronde and Kamo, 2000), which immediately predates the regional metamorphism and contemporaneous crustal magmatism in the BGB (Kamo and Davis, 1994; Schoene et al., 2008). Of particular interest here, the Inyoni shear zone is interpreted as a west or northwest vergent subduction zone (Moyen et al., 2006; Kisters et al., 2010; Cutts et al., 2014, 2015).

In an alternative interpretation, referred to as the volcanic plateau model (Van Kranendonk, 2011; Van Kranendonk et al., 2014), the BGB is argued to represent structural remnants of a thick pile of greenstones that were erupted onto older continental basement and/or older mafic crust. In this scenario the crust was affected by partial convective overturn, whereby dense greenstones sank into partially molten middle crust at *c.* 3.26–3.22 Ga, accompanied by the intrusion of *syn*-kinematic granitoids and the deposition of predominantly clastic sedimentary rocks in developing synclines (Van Kranendonk, 2011). The argument against a subduction setting is based principally on the subvertical rather than subhorizonal structures and the variable metamorphic conditions in relation to the structural position of rocks relative to the basement

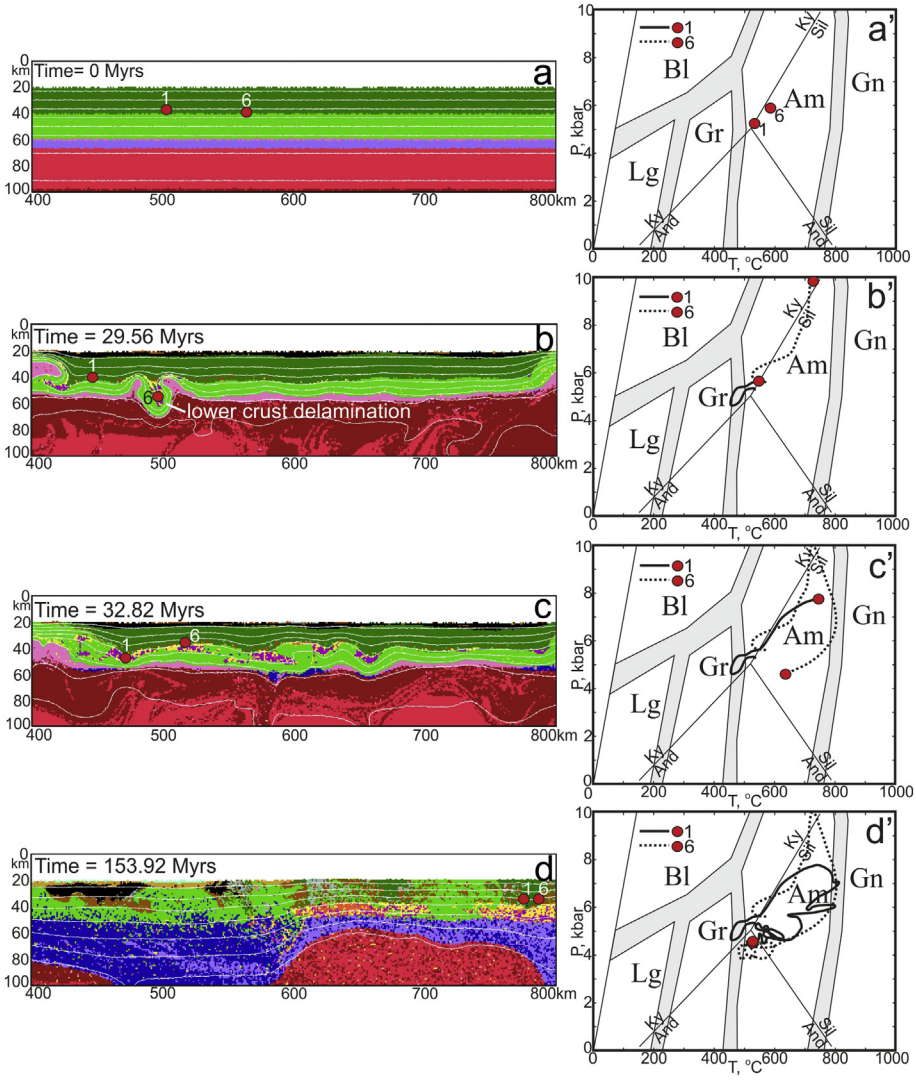

Fig. 6. A time series comprising four representative snapshots from the experiment (400 × 100 km sections of the original 1000 × 500 km model) with *P–T* diagrams to show the development of the *P–T–t* paths (a′–d′) for markers 1 and 6 (red circles, from Fig. 3), which are located in greenstones close to the dome margins, during the formation of the granite–greenstone-like crust.

domes (Van Kranendonk, 2011; Van Kranendonk et al., 2014). In this alternative view, the Inyoni shear zone is interpreted to represent "*just another drip of relatively cool, relatively rigid greenstones into hot, ductile granitic gneisses*" (Van Kranendonk et al., 2014).

In the southern terrane, to the northeast of the Komati fault, metamorphic pressures are generally low and the metamorphic grade varies from sub-greenschist to uppermost greenschist facies, with *P–T* conditions in the range 2–5 kbar and 300–500 °C (Cloete, 1999; Grosch et al., 2012). By contrast, to the south of the Komati fault, in the Stolzburg domain, metamorphic pressures—although variable—are higher and the metamorphic grade is generally amphibolite facies, The most recent estimate of *P–T* conditions recorded in the Tjakastad schist belt was based on peak pressure phase assemblage fields on *P–T* pseudosections, which yielded *P* of 9 ± 1 kbar at *T* of 590 ± 30 °C and 8.5 ± 1 kbar and 590 ± 30 °C (samples BKC-16 and -23, respectively; Cutts et al., 2014). These results are within uncertainty of earlier work by Diener et al. (2005, 2006). In the Inyoni shear zone ~12 km to the west, avPT thermobarometry (using THERMOCALC; Powell and Holland, 2008) yielded *P–T* conditions of 12–15 kbar at *T* of 600–650 °C (Moyen et al., 2006), whereas *P–T* conditions based on the peak pressure phase assemblage field on a *P–T* pseudosection yielded *P* of >13 kbar at *T* of >650 °C (sample SL 1–6; Diener et al., 2006). However, more recent work indicates lower *P*, high *T* conditions the Inyoni shear zone, consistent with the occurrence of migmatitic garnet amphibolites (Nédélec et al., 2012). Thus, *P–T* conditions based on garnet and plagioclase compositions in the peak pressure phase assemblage field on *P–T* pseudosection for a migmatitic garnet amphibolite and a sub-solidus garnet amphibolite yielded *P* of 10–11 kbar at *T* of 650–700 °C and *P* of 9–10 kbar at *T* of 650–700 °C, respectively (Nédélec et al., 2012). There is a regional trend of increasing peak pressure to the south away from the Komati fault (Cutts et al., 2014; Diener et al., 2005, 2006), which is permissible in both the core complex model (Kisters et al., 2003) and the volcanic plateau model (Van Kranendonk, 2011; Van Kranendonk et al., 2014). Apparent thermal gradients were 65–70 °C/kbar in the Tjakastad schist belt. Although Moyen et al. (2006) argued for low apparent thermal gradients of 45–50 °C/kbar in the Inyoni shear zone to the west, the more recent data of Nédélec et al. (2012) indicate apparent thermal gradients were in the same range as those from the Tjakastad schist belt.

The age of the amphibolite facies metamorphism in the Stolzburg domain is generally taken to be *c.* 3.23 Ga, based on U-Pb zircon and titanite ages (Diener et al., 2005), only slightly younger than the age of the hypothesized collision along the Saddleback–Inyoka fault system. In addition, Cutts et al. (2014) report two U-Pb monazite ages of *c.* 3.44 and *c.* 3.19 Ga, and ages from garnet of *c.* 3.23 (Lu-Hf) and *c.* 3.02 (Sm-Nd) Ga from the central Stolzburg domain. The earlier metamorphic event, which included growth of andalusite at lower amphibolite facies, was

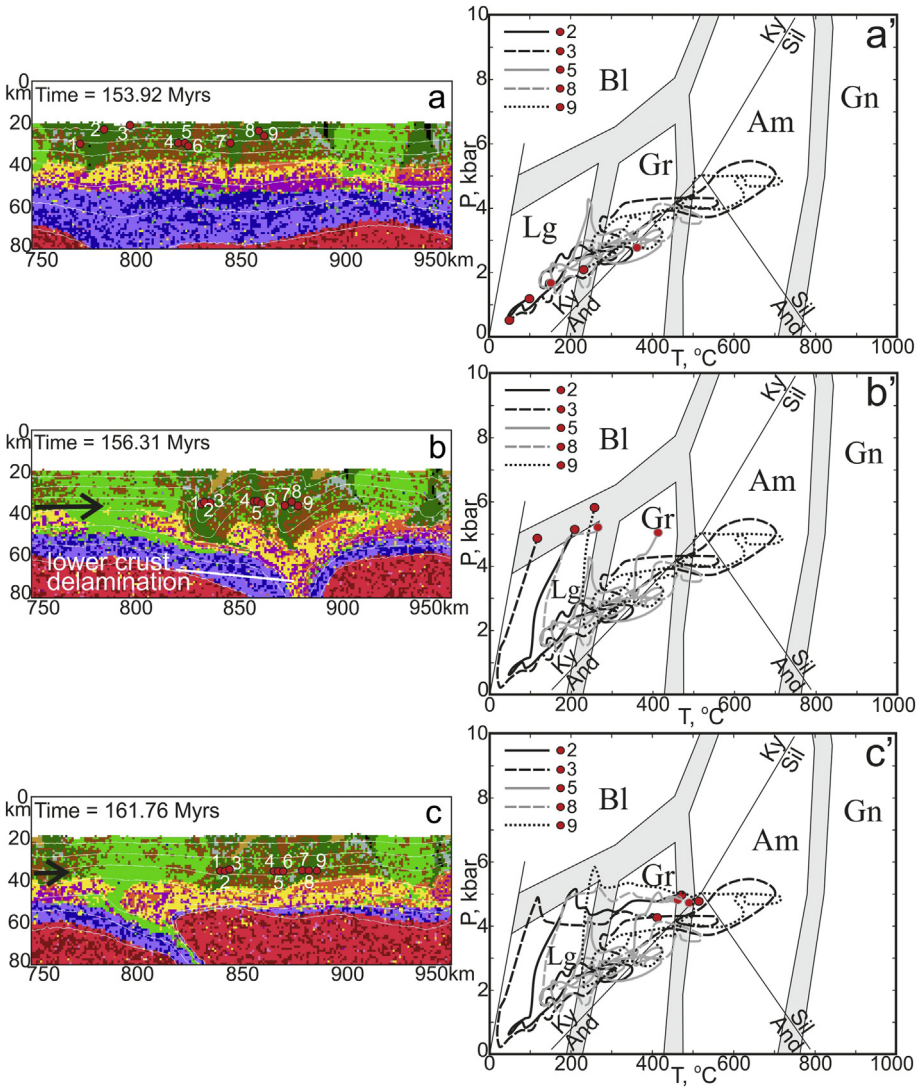

Fig. 7. A time series comprising three representative snapshots from the experiment (200 × 80 km sections of the original 1000 × 500 km model; (a–c)) with *P–T* diagrams to show the evolution of *P–T* conditions (a′–c′) for five selected markers (red circles) during deformation of the initial dome-and-keel structured granite–greenstone-like crust (shown in (a)) by a shortening/lower crustal delamination event (b,c). The *P–T–t* paths in (a') record the evolution of the markers from the beginning of the experiment up to 153.92 Myrs (snapshot (a)). See text for further explanation.

identified in sample BKC-8 from the north-eastern margin of the Stolzburg domain between the Theespruit pluton and the Komati fault (Cutts et al., 2014), and may have been related to emplacement of the Theespruit pluton. The age of *c.* 3.23 Ga is also considered to be the age of doming of the 3.55–3.45 Ga gneisses in the Stolzburg domain (Cutts et al., 2015), which is consistent with two zircon ages of *c.* 3.24 and *c.* 3.26 Ga from a younger phase of the Stolzburg pluton (Kamo and Davis, 1994), and a precise zircon age of 3.216 Ga for a late synkinematic granite sheet within a greenstone raft in the Stolzburg pluton (Schoene et al., 2008).

South of the Komati fault, the main composite tectonite fabric in the schists is steeply oriented with a strong, generally steeply south- to east-southeast-plunging mineral elongation lineation (Diener et al., 2005; Kisters et al., 2003; Van Kranendonk et al., 2009). From south to north across the schists, strong amphibolite facies prolate fabrics that record high constrictional strain are overprinted by greenschist facies fabrics that are generally close to plane strain. C′–S relations in these mylonitic rocks record kinematics consistent with dextral oblique-slip displacement, indicating that the BGGB north of the Komati fault has been displaced down relative to the Stolzburg domain (Diener et al., 2005; Kisters et al., 2003; Van Kranendonk et al., 2009). These structures have been argued to be consistent with the both core complex model (Kisters et al., 2003) and the volcanic plateau model (Van Kranendonk et al., 2014).

2.3. Summary

In summary, based on the geological evidence there is still no consensus on the geodynamic setting for the evolution of either the EPT or the BGGB. In particular, metamorphic *P–T–t* paths and apparent thermal gradients have been argued to be consistent with both subduction and sagduction for each domain. However, there are only a few studies that address the *P–T–t* evolution of markers located in different tectonic settings in experiments based on numerical modeling for upper mantle conditions appropriate to the Precambrian, whether related to subduction and plate tectonics or non-uniformitarian geodynamic regimes (François et al., 2014; Sizova et al., 2014). Therefore, in this study we undertake a detailed analysis of *P–T–t* paths recorded by markers in the reference experiment of Sizova et al. (2015). We use the results to assess whether the metamorphic *P–T–t* paths retrieved from the EPT or the BGGB are compatible with the type of non-uniformitarian geodynamic regime that could have prevailed on the early Earth.

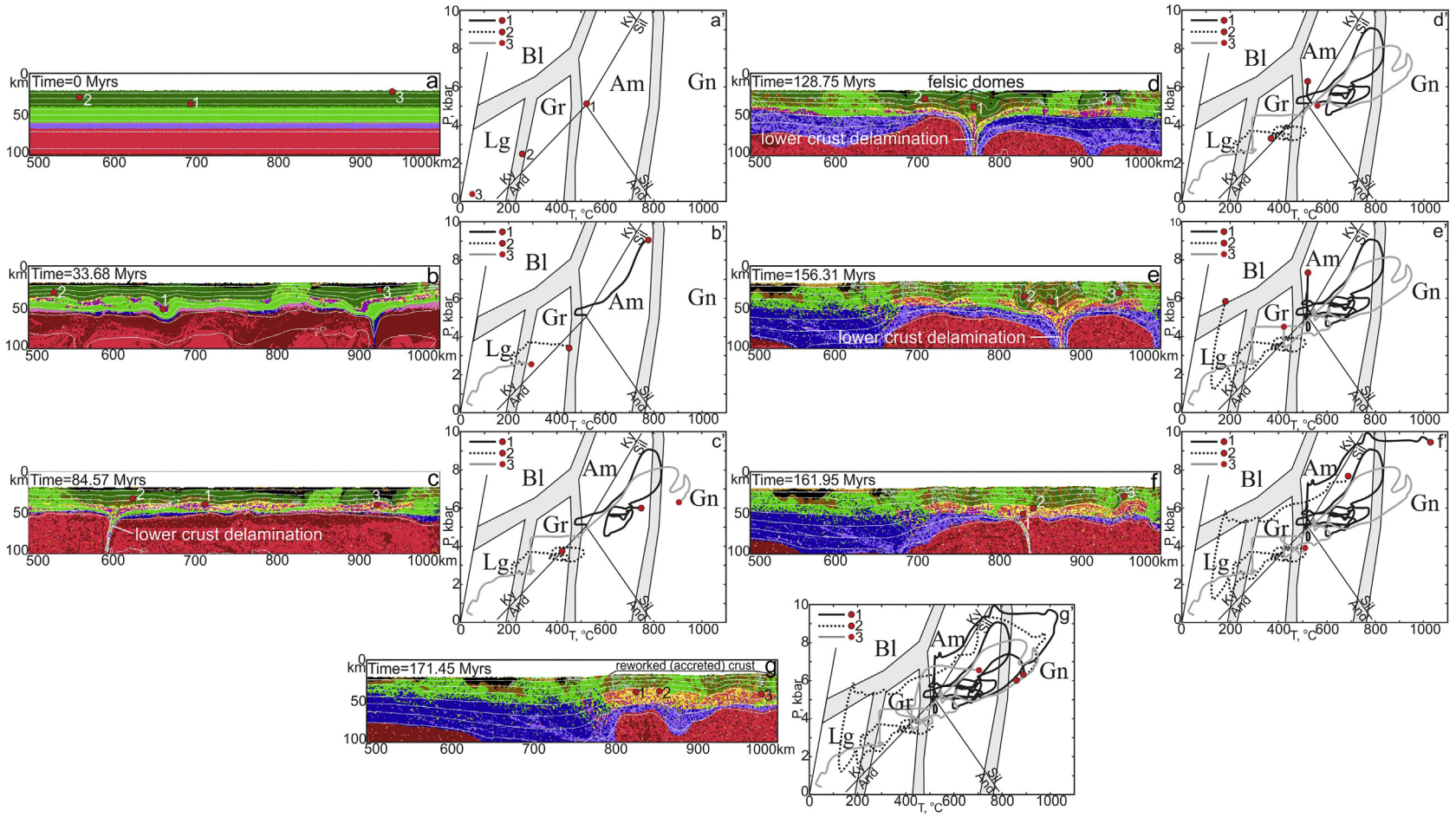

Fig. 8. A time series comprising seven representative snapshots from the experiment (500 × 100 km sections of the original 1000 × 500 km model; (a–g)) with *P–T* diagrams with to show the development of the *P–T–t* paths (a′–g′) for three markers (red circles) during the evolution from granite-greenstone-like crust to reworked (accreted) crust. See text for further explanation.

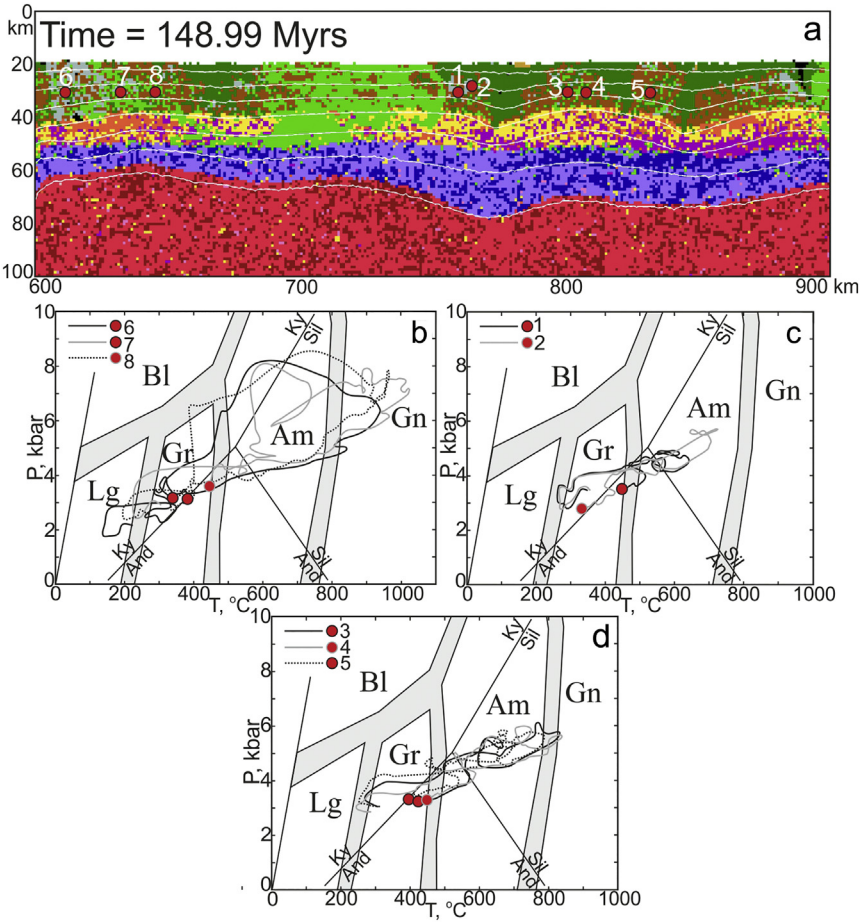

Fig. 9. A representative snapshot from the experiment (300 × 100 km section of the original 1000 × 500 km model; (a)) at 148.99 Myrs with *P–T* diagrams (b–d) to show the *P–T–t* paths for 8 markers (red circles) now located in enclaves within the felsic domes.

3. Numerical modeling

For this study we analyzed markers embedded in the petrological–thermomechanical numerical model used for the reference experiment of Sizova et al. (2015) to investigate the relationship between the different tectonic settings in the experiment and the metamorphic *P–T–t* paths traced by the markers.

3.1. The numerical model

The numerical model is based on the I2VIS code of Gerya and Yuen (2003a). Details of the numerical model and the experiment are described in Sizova et al. (2015), which builds upon the previous work of Gerya and Yuen (2003a, 2003b), Sizova et al. (2010, 2014) and Vogt et al. (2012). An important feature of the model is that it evolves self-consistently according to spontaneous material redistribution in response to contrasts in densities and viscosities intrinsic to different model lithologies, and those induced by temperature variations, partial melting, melt extraction, melt crystallization, mantle depletion and crustal eclogitization. Some relevant points of nomenclature for the current article are summarized below.

Melt extracted from the mantle that reaches the surface is represented as *hydrated basalt* in the experiment, due to interaction with sea water when erupted as volcanics at the surface (black in Fig. 3, analogous to the initial hydrated basalt crust, which is green in Fig. 3; this lithology melts at the wet basalt solidus). Mantle-derived melt emplaced at depth in the crust, it is represented as *dry basalt* (pink when melt and light-green when crystallized in Fig. 3; this lithology melts at the dry basalt solidus). All intermediate to felsic lithologies derived by melting from the mafic substrates are collectively called *dacites* (cf. Vogt et al., 2012). We apply a low extraction threshold of 75% crystallization of the dry basalt melt, which is intrusive into the crust, before drainage of the fractionated more felsic melts occurs. These fractionated melts are labeled dacite from dry basalt (yellow in Fig. 3, dark brown if crystallized) when emplaced in the crust or erupted at the surface. We also consider partial melting of the dry basalt (light green in Fig.3; equivalent to gabbro forming the lower layer of the initial crust or the crystallized intrusive dry basaltic melts extracted from the mantle). However, we do not separate the melts fractionated from cooling and crystallizing dry basaltic melt and the melts derived from partial melting of dry basalt during heating (melt-bearing dry basalt), and both types of felsic melt are referred to as *dacite*, and further in the text as *felsic crust*. In this simplified crustal differentiation model, we do not consider melt drainage from melt-bearing felsic and sedimentary rocks, both of which would produce more K-rich granitic compositions.

3.2. The reference experiment

For this study, we use the reference experiment of Sizova et al. (2015). The initial model configuration is simple (Fig. 3) and comprises a relatively thick primordial mafic crust (40 km) represented by 20 km of hydrothermally altered basalt (hydrated basalt) on top of 20 km of gabbro (dry basalt). The asthenospheric mantle temperature is increased by 250 °C compared to the present-day value, which is taken to be 1340 °C. Gravitational redistribution of materials in the crust and mantle

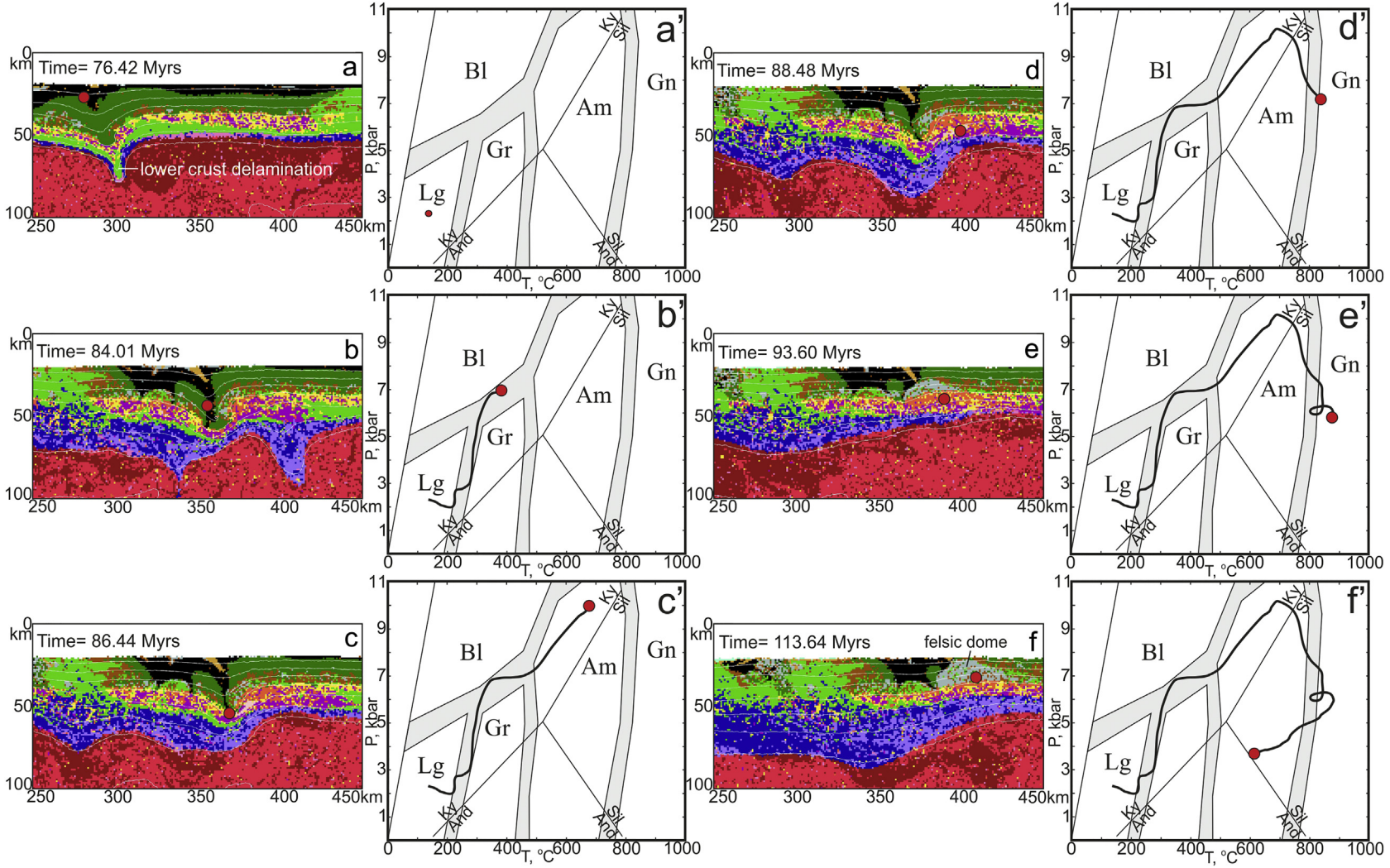

Fig. 10. A time series comprising six representative snapshots from the experiment (200 × 100 km sections of the original 1000 × 500 km model; (a–f)) with *P–T* diagrams (a′–f′) to show the development of the *P–T–t* paths (a′–f′) for a marker in basalt (red circle) that subsequently appears as an enclave within a felsic dome.

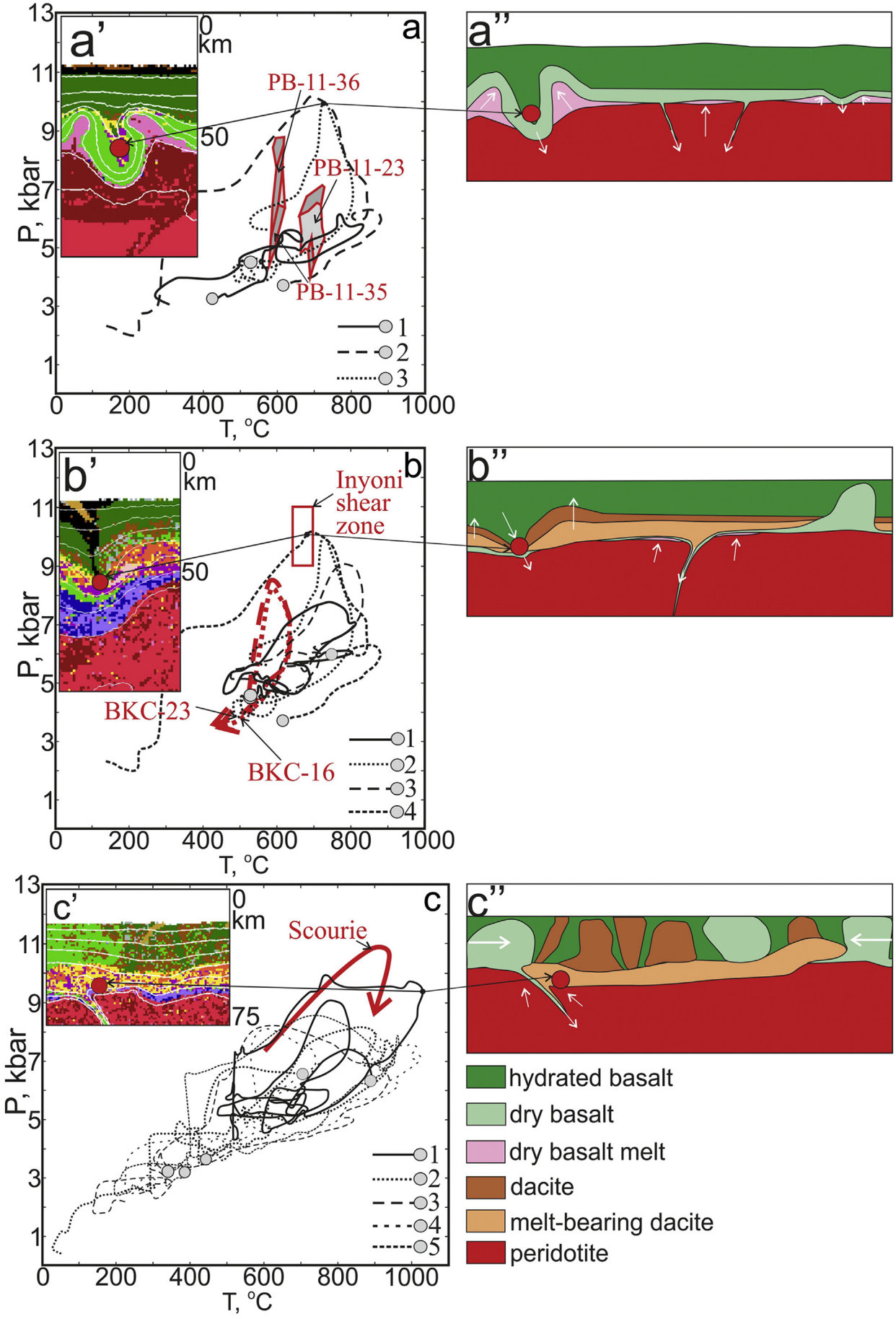
a'
0
km
50
a
a''
PB-11-36
PB-11-23
PB-11-35
P, kbar
T, °C
1
2
3
b'
0
km
50
b
b''
Inyoni
shear
zone
BKC-23
BKC-16
4
c'
0
km
75
c
c''
Scourie
5
hydrated basalt
dry basalt
dry basalt melt
dacite
melt-bearing dacite
peridotite

begins after a few million years. These Rayleigh-Taylor type instabilities continue throughout almost the entire experiment (ca. 200 Ma).

On timescales of tens to hundreds of millions of years, various tectono-magmatic processes gradually rework the primordial mafic crust into a more felsic continental crust (Fig. 4a, b). A layer of dacite is continuously produced in the middle–lower crust. This undergoes periodic re-melting from the bottom, which leads to the formation of felsic domes that rise to penetrate the overlying mafic crust. As the domes rise, the mafic crust is moved downward to stabilize the unstable structure created by the density inversion. This process forms the archetypal dome-and-keel structure characteristic of Archean granite–greenstone domains (e.g. François et al., 2014; Van Kranendonk, 2011). These granite–greenstone domains overly a more mafic, high-grade lower crust. During further evolution of the experiment, these continent-like crustal blocks undergo shortening and amalgamation due to pushing from the left, where a new spreading center has progressively produced an oceanic plate (Fig. 4b). The shortening is terminated by short-lived subduction of the oceanic plate under the continent-like crustal block (Fig. 4c). The resulting reworked (accreted) crust represents a strongly deformed mix of felsic (50–60%) and mafic (40–50%) domains without well-defined boundaries for the intrusive bodies and is continental (Fig. 4c). Thus, during the evolution of the experiment two distinct types of continent-like crust are developed sequentially: (1) a pristine granite–greenstone-like crust with dome-and-keel geometry formed over delaminating–upwelling mantle, which was mostly subjected to vertical tectonics processes (Fig. 4b); and, (2) a reworked (accreted) crust comprising strongly deformed granite–greenstone-like crust and subduction-related sequences, which was subjected to both vertical tectonics processes and strong horizontal shortening (Fig. 4c).

3.3. Choice of markers for model P–T–t paths

For a proper assessment of the results of the experiment it is important to compare the natural metamorphic data not only with the final *P–T* values defined by markers at the end of the experiment, but also with the *P–T–t* paths tracked by those markers during the geodynamic evolution of the experiment, and, in particular, with the peak *P–T* values achieved along those paths. For this purpose, several series of markers were selected in the greenstones to trace the change in *P–T* values during the experiment. The errors associated with the *P–T* values retrieved from the experiment are ± 5 °C and ± 0.1 kbar, which are mainly related to interpolation errors from the Eulerian grid to the Lagrangian markers.

As discussed above, there are large pressure variations in both the EPT and the southern terrane of the BGB, although much of this variation relates to the higher pressures associated with high strain rocks along the margins of domes. Away from the dome margins, the pressures correspond to mid-crustal conditions—generally 2–5 kbar (Cloete, 1999; Grosch et al., 2012; Terabayashi et al., 2003), which approximates an erosion level of ~7–17 km (assuming an average crustal density of 2700–3000 kg m^{-3}). This range corresponds well with the average erosion level in the Archean Superior Province, where most of the exposed crust records pressures of 3–5 kbar, equivalent to ~10–17 km depth, with only limited areas of crust where the pressures are lower or higher (Percival et al., 2012, their Fig. 7). Similarly, metamorphic pressures over much of the Archean Eastern Yilgarn craton lie in the range 3 to 5 kbar, with only localized burial to higher pressures (Goscombe et al., 2009, their Fig. 155).

Based on this analysis, we concentrate on markers with endpoints located at a depth of 10–15 km in the particular time-slice snapshot chosen (note that the top of the crust in the snapshots shown in the figures is located at 20 km depth due to the layer of air/water above the crust, which is a necessary component of the numerical model). For these markers, the *P–T–t* paths are traced back from the endpoint to the start of the experiment.

At a depth of 10–15 km, the blocks of granite–greenstone-like crust are composed of multiphase felsic domes 15–50 km in diameter and intervening greenstone belts (Fig. 4b). In addition to the greenstone keels, greenstone remnants also occur in the reworked (accreted) crust and as numerous enclaves in the felsic domes (Fig. 4c). We will discuss the *P–T–t* evolution separately for selected markers located in each of these three types of greenstone.

4. The *P–T–t* record of markers in the experiment

For the Archean, when the ambient mantle temperature and heat production were higher (Labrosse and Jaupart, 2007; Korenaga, 2013), calculated pressures for a weak continental crust should approximate load pressure (i.e. differential stress and tectonic overpressure may be neglected in converting pressure to depth or vice versa). This is assumed to be true for the granite–greenstone-like crust in the experiment used for this study.

4.1. P–T–t paths for greenstone keels in the granite–greenstone-like crust

For hydrated basalt forming the greenstone keels between felsic domes in one block of granite–greenstone-like crust we analyzed selected markers located at two depths—10 km and 15 km below the top of the crust (i.e. at 30 km and 35 km depth in Fig. 5a). Markers in the interior of greenstone keels (13, 14, 17, 18 and 21 at 30 km depth and 2, 3, 4, 7, 9 and 10 at 35 km depth in Fig. 5a) record endpoint *P–T* values equivalent to either greenschist (30 km) or amphibolite (35 km) facies metamorphism (red dots at the termination of *P–T* paths in Fig. 5b,d), reaching their final values of ~3 kbar at 300–400 °C (Fig. 5b) or 4.5 kbar at 500–550 °C at 153.92 Myrs (Fig. 5d). The metamorphic evolution recorded by these markers is related to their downward movement correlated with simultaneously rising domes on either side, and the endpoint *P–T* values are similar to the metamorphic peak.

By contrast, markers closer to the dome margins (12, 15, 16, 19, 20 and 22 at 30 km depth and 1, 5, 6, 8 and 11 at 35 km depth in Fig. 5a) are characterized by *P–T* paths significantly different to those from the interior of the greenstone keels (Fig. 5c, e). For these markers, the peak metamorphic *P–T* values occurred during the early stages of the *P–T* evolution due to local crustal thickening, lower crust delamination events, and subsequent heating from mantle upwellings (Fig. 6). For example, markers 1 and 6 were buried to model depths of approximately 45–55 km by overplating of basaltic melts and local crustal thickening associated with lower crustal delamination (Fig. 6b, c). At this depth they underwent upper-amphibolite facies metamorphism reaching *P–T* values of 7.7 kbar at 750 °C and 10 kbar at 720 °C, respectively (Fig. 6b′, c′). Due to conductive heating from the underlying dry basaltic melts

Fig. 11. Comparison between natural examples of *P–T* paths from the East Pilbara Terrane, Australia (a), the Barberton greenstone belt, South Africa (b) and the Lewisian complex, Scotland (c) and exemplar model *P–T* paths from the experiment. (a) *P–T* fields for samples PB-11-35/36 and PB-11-23 (from François et al., 2014; see Fig. 1), and *P–T* paths for marker 3 from Fig. 9d (line 1), the marker from Fig. 10 (line 2), and marker 6 from Fig. 6 (line 3). (b) *P–T* paths for samples BKC-16 and 23 from the Tjakastad schist belt (Cutts et al., 2014; see Fig. 2) and *P–T* data from the Inyoni shear zone (Nédélec et al., 2012), and *P–T* paths for markers 1 and 6 from Fig. 6 (lines 1 and 2, respectively) and marker 1 from Fig. 8c (line 3), and the marker from Fig. 10 (line 4). (c) *P–T* path for metapyroxenite and metagabbro (from Johnson and White, 2011), and markers 1 and 3 from Fig. 8 (lines 1 and 2, respectively) and markers 6, 7 and 8 from Fig. 9 (lines 3, 4, and 5, respectively). (a′), (b′), (c′) are representative snapshots and (a″), (b″), (c″) are simplified geodynamic sketches showing the conditions under which the selected markers reached the peak metamorphic values. (a″) Shows an intermediate stage during the formation of the granite–greenstone-like crust in which gravitational redistribution has led to the formation of basaltic magmas underplating the crust, which accumulate and rise upwards with the simultaneous sinking of mafic middle and lower crust. (b″) Shows the simultaneous sinking of mafic upper and middle crust between rising felsic domes on either side; the rising domes may incorporate remnants of the sinking greenstones as enclaves. (c″) Shows reworking of the granite–greenstone-like crust by shortening and periodic remelting of the middle and lower crust by heating from the bottom as drips of eclogitic lower crust sink into the melt-bearing peridotite of the underlying mantle.

the markers reached the amphibolite-to-granulite facies transition, achieving maximum temperatures of 800 °C (Fig. 6c′, d′). Subsequently, the markers were brought to the middle crust by rising felsic domes, with endpoints at lower amphibolite facies conditions and insignificant differences in final *P–T* values. Concurrently, neighboring domes were gradually rising over a period of 50–60 Myrs until the time-slice snapshot shown in Figs. 5a/6d. Thus, markers close to the dome margins record clockwise *P–T–t* paths.

Up to 153.92 Myrs in the experiment (Fig. 5a), the granite–greenstone-like crust with dome-and-keel structures was gradually produced by reworking of mafic crust during mantle upwelling–crustal delamination events. However, the progressive shortening induced by the episodic opening of a spreading center on the left side of the model (Fig. 4b) led to thickening of the initial granite–greenstone-like crust (Fig. 7a), first producing a transitional type of crust with deformed felsic domes (Fig. 7c), before finally producing the reworked (accreted) crust, where distinct domes can no longer be distinguished. During shortening and simultaneous delamination of the lower crust, the felsic domes became deformed, especially close to their margins, while the intervening greenstone keels largely sank (sagducted) and gradually become incorporated into the partially molten lower crustal layer (Fig. 7). It is important to note that during formation of the granite–greenstone-like crust in the experiment, crustal overturns, in which domes rose and greenstones sank, occurred very slowly, taking up to 100 million years. All faster material redistributions in the crust, those up to 30 million years in duration, were strongly connected to lower crustal delamination events, which pulled down the greenstone keels more intensively until detachment (e.g. Fig. 7b).

Greenstones with endpoints at ~15 km depth in the transitional crust (35 km in Fig. 7c) started at shallower crustal levels, but have experienced a long metamorphic evolution related to several (partial) crustal overturn events (Fig. 7a′). As a consequence, the peak metamorphic conditions reached by these markers were achieved during the early stages of the *P–T* evolution, when the markers were buried into the middle/lower crust where they underwent conductive heating from the underplated basaltic melts. Subsequently, these markers were exhumed to upper crustal levels before taking part in the crustal overturn shown in Fig. 7. As a result, these markers followed a second clockwise *P–T–t* loop superimposed on the earlier *P–T–t* evolution, with endpoints in the middle crust at upper greenschist to lower amphibolite facies conditions (Fig. 7b′, c′). Ongoing shortening causes further sinking of these greenstone keels until finally they break up into the partially molten layer below.

4.2. P–T–t paths for greenstone relics in the reworked (accreted) crust

Markers in greenstone relics with endpoints at ~20 km depth below the top of the crust (~40 km depth in the experiment) at 171.45 Myrs are located within the partially molten felsic layer of the reworked (accreted) crust at upper amphibolite to granulite facies metamorphic conditions (Fig. 8). Prior to this, the metamorphic evolution was either simple, showing one or two stages of metamorphic overprinting, such as markers 2 and 3 in Fig. 8, or more complex, involving several metamorphic cycles, as, for example, marker 1 in Fig. 8.

Markers initially located in the upper and middle crust were usually buried to deeper levels by local crustal thickening and delamination of the lower crust, and reached metamorphic conditions anywhere from upper greenschist to granulite facies (Fig. 8b, c). At this stage, the markers underwent conductive heating by episodic underplating of basaltic melts and upwelling of hotter mantle (Fig. 8c), after which they were moved towards the surface by rising domes (e.g. marker 3 in Fig. 8d). Later shortening and lower crustal delamination events were able to bury the greenstones again, possibly close to the partially molten felsic layer (e.g. marker 1 in Fig. 8d). Subsequently, some greenstones were incorporated into rising domes and then buried once more during the next episode of shortening and delamination of the lower crust (e.g. markers 1 and 2 in Fig. 8e).

It is clear that the latest crustal overturn may not have been the one responsible for the peak *P–T* values achieved by the markers. As an example, we follow marker 3, which reached granulite facies conditions within the partial molten felsic layer at 84.57 Myrs (marker 3 in Fig. 8c). Subsequently, it was brought upwards by the surrounding felsic crust and then became involved in another shortening/delamination event accompanied by partial crustal overturn. This time the surrounding felsic crust did not allow the greenstone marker to sink deep, and the second stage of metamorphic overprinting reached only upper amphibolite facies (marker 3 in Fig. 8g).

4.3. P–T–t paths for greenstone enclaves in felsic domes

In the experiment, a majority of the greenstone enclaves are located in the felsic domes; these greenstones are characterized by slightly different *P–T–t* paths. At any particular depth, the metamorphic *P–T* values recorded by markers in the enclaves do not show any regular zonation across the domes, and the grade of metamorphism is correlated only with depth in the dome. Thus, markers in enclaves in the upper parts of the domes record amphibolite facies peak metamorphic conditions (*P–T* values of 4.5–5.5 kbar at 600–700 °C, Fig. 9c), whereas those in the deeper parts are characterized by granulite facies peak metamorphic conditions (*P–T* values of ~7 kbar at 900–1000 °C, Fig. 9b). Fig. 9d shows the intermediate case. All *P–T–t* paths are clockwise and all have endpoints in the greenschist facies.

A typical *P–T–t* path recorded by a marker in an enclave from the interior of a dome is shown in Fig. 10. This marker was located in hydrated basalt at the top of the crust and was initially buried by a crustal shortening/lower crustal delamination event to a depth of approximately 25 km (45 km in the model, see Fig. 10b). With further burial to the maximum *P* value (Fig. 10c′) it became incorporated into the partially molten lower-crustal layer, where it underwent conductive heating to the maximum *T* value during initial decompression (Fig. 10d'), before final exhumation towards the surface within a felsic dome (Fig. 10e–f). In this particular example, the crustal overturn event lasted approximately 30 Myrs, from the maximum depth of burial (Fig. 10c) until the endpoint in the amphibolite facies middle crust (Fig. 10f).

5. Discussion

Although the geological record preserved from the early Archean is fragmentary, it is notable that blueschists, a characteristic metamorphic rock associated with Phanerozoic subduction, are not found (Brown, 2014). This observation suggests that the higher ambient mantle temperatures at that time may have precluded modern-style plate tectonics (Sizova et al., 2010; Gerya, 2014). If so, what was the geodynamic regime in the early Archean?

There are several examples of numerical modeling studies that have tried to explain the formation and modification of the first felsic crust on Earth (e.g. Johnson et al., 2014; Moore and Webb, 2013; Moyen and Van Hunen, 2012; Rozel et al., 2017; Van Thienen and Van den Berg, 2004). However, there are almost no studies applicable to the direct comparison of the magmatic–metamorphic record of the early Archean crust with those predicted by numerical modeling experiments, although the work of François et al. (2014) is a notable exception.

In this study we have extracted the *P–T–t* paths for markers from a variety of tectonic settings in the reference experiment of Sizova et al. (2015). Next we compare the *P–T–t* paths traced by markers from different tectonic settings in the experiment with metamorphic *P–T–t* paths retrieved from natural Archean terranes. In making these comparisons it is important to remember that the model is set-up with a pre-existing simple layered crust. By contrast, in the natural examples, the mafic sequences comprise repeated cycles of magmatic activity over tens to several hundreds of millions of years and the felsic crust is commonly polyphase (e.g. Gardiner et al., 2017; Johnson et al., 2017; Rozel et al., 2017).

In the experiment, the *P–T–t* paths are traced by markers in the crust; these markers have terminal *P–T* values equivalent to depths below the top of the crust of 10 or 15 km, which is similar to the erosion level of many Archean cratons. Although we identify similarities between the results from the experiment and the natural examples, we acknowledge that the complexity of the natural examples and the finer details of the geology that vary from one example another will not be reproduced by our experimental approach. We also acknowledge that the depth of erosion varies from craton to craton and across cratons. Thus, our study is only the first step in investigating whether non-uniformitarian processes could have been involved in the generation and metamorphic evolution of granite–greenstone crust.

The contrast between the *P–T–t* paths of greenstone belt interiors and their margins near the surrounding felsic domes registered in the experiment is consistent with the metamorphic record of greenstones within the East Pilbara Terrane (EPT). In the EPT, the greenstones in the interior of synformal belts are generally undeformed and characterized by very low-pressure prehnite–pumpellyite to greenschist facies metamorphism with *P–T* conditions of <400 °C at very low pressure (Kitajima et al., 2001; Terabayashi et al., 2003). Thus, these greenstones were always in the upper crust at shallower levels than markers in Fig. 5b. By contrast, those near the margins of the belts against the basement domes are generally more highly strained and characterized by amphibolite facies metamorphism, including examples of sillimanite replacing kyanite that are consistent with clockwise *P–T–t* paths (Delor et al., 1991; Collins and Van Kranendonk, 1999; François et al., 2014). In Fig. 11a we plot *P–T* fields for samples at two locations on a traverse from south to north from Trig Well in the Warrawoona greenstone belt into the Mount Edgar dome, and for an enclave of garnet-bearing migmatite from within the Mount Edgar dome (from François et al., 2014; see Fig. 1). We compare these data with exemplar model *P–T* paths from a greenstone belt margin (marker 6 from Figs. 5e and 6) and two enclaves (marker 3 from Fig. 9d and the marker from Fig. 10). The two samples from Trig Well yield *P* decreasing from ~9 to <5 kbar at *T* of 600 ± 20 °C, whereas the enclave within the Mount Edgar dome records *P–T* conditions of ~5.5 kbar at ~690 °C (François et al., 2014). Although the model *P–T* paths are hotter than the metamorphic data from the EPT, the clockwise paths are similar in overall shape to those implied by the natural examples. Whether the difference in maximum temperatures achieved between the markers in the experiment and the metamorphic data are due to an underestimate of the *P–T* conditions from the EPT samples cannot be assessed with the limited information about the methods used provided in François et al. (2014).

In the EPT two ages of metamorphism are identified at *c.* 3.443 Ga and *c.* 3.312 Ga (François et al., 2014), which correspond to the older gneissic (3.47–3.43 Ga) and younger granodiorite (3.32–3.29 Ga) components of the Mount Edgar dome (Williams and Collins, 1990; Kloppenburg, 2003). Thus, the overall timescale for the evolution of the Mount Edgar dome and the greenstones at the margin in the Warrawoona greenstone belt (131 Myrs) is similar to that for samples at the margins of the greenstone keels in the experiment (121–124 Myrs, Fig. 6b/c to d). The evidence of multiple tectono-magmatic/metamorphic events spanning long timescales is consistent with geochemical evidence for multiple recycling of mafic crust during the production of the TTG gneisses within the EPT (Gardiner et al., 2017; Johnson et al., 2017).

A similar dependence of *P–T* conditions on position relative to the felsic domes is present in the greenstones and schists of the Barberton granite–greenstone belt (BGB). For example, within the southern terrane of the BGB the metamorphic grade increases from sub-greenschist to greenschist facies north of the Komati fault (Cloete, 1999; Grosch et al., 2012), and then to amphibolite facies to the south and southwest of the Komati fault across the Stolzburg and Tjakastad schist belts, reaching *P–T* conditions of ~9 kbar at ~590 °C in the Tjakastad schists (Cutts et al., 2014) and 9–11 kbar at 650–700 °C within the Inyoni shear zone (Nédélec et al., 2012). The *P–T* paths are clockwise and analogous to those recorded in the experiment by markers located across the greenstone belts (markers 1 and 6 in Figs. 5e and 6, and marker 1 in Fig. 8c) and in some enclaves (e.g. Fig. 10). Although, the peak *P–T* values are hotter in the experiment (Fig. 11b), this difference likely could be mediated in an experiment explicitly designed for the crustal profile of the BGB.

Similar to the EPT, the age of the amphibolite facies metamorphism is late in the evolution of the BGB at *c.* 3.23 Ga (Cutts et al., 2014; Diener et al., 2005; Dziggel et al., 2005), which is also considered to be the age of doming, whatever the cause, of the gneisses in the Stolzburg domain (Cutts et al., 2015). Cutts et al. (2014) estimate the time spent at elevated temperatures by the greenstone belt samples plotted in Fig. 11b was on the order of 30 Myrs, broadly comparable with the timescale for marker 6 in Fig. 6, but faster than the timescale for marker 1 in Fig. 8a–c. The precursors of the gneisses were emplaced in the interval 3.55–3.45 Ga (Kamo and Davis, 1994) and were associated with lower amphibolite facies metamorphism at 3.44 Ga (Cutts et al., 2014). Thus, the overall timescale of crustal evolution from the emplacement of the Stolzburg pluton protoliths to the doming event and the associated metamorphism was a minimum of 220 Myrs.

In the experiment, initial convective overturn occurs due to the formation of felsic diapirs and their gradual rise as the overlying greenstones simultaneously sink. This crustal overturn is a very slow process, lasting up to 100 Myrs (e.g. Fig. 6). However, the process may be greatly accelerated by lower crustal delamination events (e.g. Fig. 8d). Sinking of the lower crust exerts a strong force that pulls down the greenstones around the domes, while the positive buoyancy of the felsic domes allows the domes to stay more or less at the same structural depth. In addition, mantle upwelling following lower crustal delamination leads to a relaxation stage (involving some extension) with crustal heating and remelting of the lower crust, maintaining the buoyancy of the domes. These processes may recycle granite–greenstone-like crust through more than one tectono-metamorphic event (Fig. 7).

Such a recycling process may be relevant to the EPT and the BGB, where older felsic plutonic complexes associated with early metamorphism underwent doming associated with the dominant tectono-metamorphic event some 100 to 200 Myrs later, as discussed above. Coupled shortening associated with lower crustal delamination provokes deformation within the crust. As a result, the sinking greenstone belt generates strong deformation of the dome margins, while the interior remains more or less unaffected (Fig. 5). These predictions are in good agreement with structures in both the EPT and the BGB, where the interior of the felsic domes remain largely undeformed, while the dome margins and the adjacent greenstones are characterized by subvertical ductile shear zones (Collins and Van Kranendonk, 1999; Kisters et al., 2003). Such structures have been interpreted as evidence of partial convective overturn in both the EPT and the BGB (Van Kranendonk et al., 2004, 2014, 2014; Van Kranendonk, 2011), similar to results from experiments using numerical modeling (Dixon and Summers, 1983).

In the experiment, although coupled shortening and delamination of the lower crust can greatly accelerate the process of greenstone sinking, the time needed for a full crustal overturn, where the greenstone is first buried and then exhumed to the middle-lower crust, is a minimum of 30 Myrs (e.g. Figs. 9, 10). This contrasts with the results of François et al. (2014) for the EPT based on a simple model of convective overturn, which predicts a minimum time for burial and exhumation of the greenstones of <5 Myrs. The most time-consuming component of the convective overturn in our experiment is the slow rise of the felsic diapirs. In our experiment the lower crustal partially molten layer is a hybrid of dacitic and basaltic melts, with the result that its buoyancy is less than the buoyancy of simple felsic layer as used in the model of François et al. (2014). We infer that the longer exhumation times in our experiment may be due to the lower buoyancy contrast between the hybrid partially molten lower crustal layer and the greenstones compared with the model of François et al. (2014).

The development of the greenstone–granite-like crust in the experiment generates a wide range of thermal gradients (50–150 °C/kbar; e.g.

Figs. 5, 7) that are similar to those determined by François et al. (2014); 40–175 °C/kbar). Similarly, the thermal gradients derived for the reworked (accreted) crust are mostly in the range 75 to 100 °C/km (Fig. 8). The range of values from the experiment extends down to the apparent thermal gradients of 45–50 °C/kbar derived from the Inyoni shear zone that Moyen et al. (2006) inferred "*strongly suggest that lithospheric subduction was functioning as early as 3.2 Gyr ago before present*." However, more recent data (Nédélec et al., 2012) suggest that apparent thermal gradients in the Inyoni shear zone were higher, in the range 65 to 70 °C/kbar. Thus, our results support the conclusion of François et al. (2014), that a relatively low apparent thermal gradient imprinted in metamorphic rocks from the early Archean cannot be used as a robust discriminant of tectonic setting.

In the experiment, ongoing shortening and further convective overturns that affect the greenstone–granite-like crust result in the greenstones sinking deeper into the partially molten lower crustal layer, where they are overprinted by granulite (amphibolite) facies metamorphism as they become incorporated into the felsic crust as greenstone relics within the reworked (accreted) crust (Fig. 8). Such highly deformed relict greenstones are typical of natural high-grade grey gneiss complexes (e.g. the Akilia association supracrustal rocks within the early Archean Itsaq gneiss complex of southern West Greenland (Griffin et al., 1980; Nutman et al., 2002)), although the details of the *P–T–t* paths are generally unknown. In a series of recent studies, Johnson and White (2011) and Johnson et al. (2012, 2016) investigated the origin and metamorphism of mafic–ultramafic bodies that occur throughout the central region of the Archean Lewisian Complex of NW Scotland. In these bodies, metagabbros show evidence of partial melting during ultrahigh temperature granulite facies metamorphism (Johnson et al., 2012), analogous to occurrences in our experiment (Figs. 8, 9, 10). In Fig. 11c we compare the *P–T* path determined by Johnson and White (2011) for the mafic–ultramafic body at Scourie in the Lewisian complex with *P–T* paths for reworked (accreted) crust (markers 1 and 3 in Fig. 8) and enclaves (markers 6, 7 and 8 in Fig. 9). In this case, the model *P–T* paths are generally comparable with those from nature. Furthermore, Johnson et al. (2016) postulated that mafic–ultramafic bodies in the Lewisian complex represent remnants of intracratonic greenstone belts that sank into the deep crust.

6. Conclusions

We analyzed the *P–T–t* paths of material particles (markers) in greenstones in granite–greenstone-like crust from the reference experiment of Sizova et al. (2015), which used a 2D coupled petrological–thermomechanical tectono-magmatic numerical model, constrained using information from the geological record, with initial conditions appropriate to the Eoarchean–Mesoarchean. By comparison with natural examples of *P–T* and age data from the early Archean East Pilbara Terrane, part of the Pilbara craton in Western Australia, and the Barberton greenstone belt, part of the Kapvaal craton in South Africa, we demonstrated that the numerical results although hotter are similar to the natural *P–T* paths, timescales and thermal gradients. The granite–greenstone crust with dome-and-keel structures produced in the experiment is similar to the crust and structure of Archean greenstone belts. The combination of similar metamorphic *P–T–t* records and structural features between the numerical model and the exemplar greenstone belts supports the idea that natural granite–greenstone crust could have formed in a regime of crustal delamination–mantle upwelling analogous to the experiment. In addition, for amphibolite-to-granulite facies supracrustal relics in a high-grade grey gneiss terrain we confirmed their possible origin as highly deformed greenstone keels that sank into the partially molten felsic lower crust. In the experiment, these relics are characterized by higher grades of metamorphism than greenstones from the granite–greenstone-like crust, which is consistent with mafic–ultramafic bodies in the Archean Lewisian Complex of NW Scotland.

The *P–T–t* records retrieved from the experiment yield a range of apparent thermal gradients that includes those from the exemplar greenstone belts and mafic–ultramafic bodies. Thus, low apparent thermal gradients in greenstone belts are not necessarily diagnostic of subduction. Similarity between the results of the numerical experiment and the metamorphic record of the Archean crust permits an intracratonic model for the formation of greenstone belts, as implied, for example, by the well-exposed unconformable basal contact of shallow-water sediments and extrusive komatiites on granitic crust in the Belingwe greenstone belt of Zimbabwe (Bickle et al., 1975). Thus, granite–greenstone crust could have developed by both vertical and horizontal tectonic processes (convective overturns) that occurred over linked sites of crustal delamination and mantle upwelling.

Acknowledgments

This work was supported by Austrian Science Fund (FWF, Lise Meitner Program, project number M 1559-N29 (E.S.)) and by an ETH-grant ETH-37_11-2 (T.G.). Simulations were performed on the ETH-Zurich Brutus cluster. We thank Tim Johnson and an anonymous reviewer, the Managing Guest Editor and Philippe Agard for comments and advice that enabled us to significantly improve this article.

References

Benn, K., Mareschal, J.-C., Condie, K.C., 2006. Archean geodynamics and environments. American Geophysical Union. Geophysical Monograph Series. 64 (320 p).
Bickle, M.J., Martin, A., Nisbet, E.G., 1975. Basaltic and peridotitic komatiltes and stromatolites above a basal unconformity in the Belingwe greenstone belt, Rhodesia. Earth Planet. Sci. Lett. 27, 155–162.
Blewett, R.S., 2002. Archaean tectonic processes: a case for horizontal shortening in the North Pilbara Granite-Greenstone Terrane, Western Australia. Precambrian Res. 113, 87–120.
Blewett, R.S., Shevchenko, S., Bell, B., 2004. The north pole dome: a non-diapiric dome in the Archaean Pilbara Craton, Western Australia. Precambrian Res. 133, 105–120.
Brown, M., 2014. The contribution of metamorphic petrology to understanding lithosphere evolution and geodynamics. Geosci. Front. 5, 553–569.
Brown, M., 2015. Paleo- to Mesoarchean polymetamorphism in the Barberton Granite-Greenstone Belt, South Africa: constraints from U-Pb monazite and Lu-Hf garnet geochronology on the tectonic processes that shaped the belt: discussion. Geol. Soc. Am. Bull. 127, 1550–1557.
Cloete, M., 1999. Aspects of volcanism and metamorphism of the Onverwacht group lava in the southwestern portion of the Barberton Greenstone Belt. Memoirs of the Geological Survey of South Africa. 84 (232 p).
Collins, W.J., Van Kranendonk, M.J., 1999. Model for the development of kyanit during partial convective overturn of Archean granite-greenstone terranes: the Pilbara Craton, Australia. J. Metamorph. Geol. 17, 145–156.
Collins, W.J., Van Kranendonk, M.J., Teyssier, C., 1998. Partial convective overturn of Archaean crust in the east Pilbara Craton, Western Australia: driving mechanisms and tectonic implications. J. Struct. Geol. 20, 1405–1424.
Cutts, C.A., Stevens, G., Hoffmann, J.E., Buick, I.S., Frei, D., Münker, C., 2014. Paleo- to Mesoarchean polymetamorphism in the Barberton Granite–Greenstone Belt, South Africa: constraints from U–Pb monazite and Lu–Hf garnet geochronology on the tectonic processes that shaped the belt. Geol. Soc. Am. Bull. 126, 251–270.
Cutts, C.A., Stevens, G., Kisters, A., 2015. Reply to "Paleo- to Mesoarchean polymetamorphism in the Barberton Granite–Greenstone Belt, South Africa: constraints from U–Pb monazite and Lu–Hf garnet geochronology on the tectonic processes that shaped the belt: discussion" by M. Brown. Geol. Soc. Am. Bull. 127, 1558–1563.
de Ronde, C.E.J., de Wit, M., 1994. The tectonic history of the Barberton greenstone belt, South Africa: 490 million years of Archean crustal evolution. Tectonics 13, 983–1005.
de Ronde, C.E.J., Kamo, S., 2000. An Archean arc-arc collisional event: a short-lived (ca. 3 Myr) episode, Weltevreden area, Barberton greenstone belt, South Africa. J. Afr. Earth Sci. 30, 219–248.
Delor, C., Burg, J.-P., Clarke, G.L., 1991. Relations diapirisme-métamorphisme dans la province du Pilbara (Australie occidentale): implications pour les régimes thermiques et tectoniques á l'Archéen. Compte Rendu de l'Acadamie des Sciences de Paris II. 312, pp. 257–263.
Diener, J.F.A., Stevens, G., Kisters, A.F.M., 2006. High-pressure–intermediate-temperature metamorphism in the southern Barberton granitoid–greenstone terrain, South Africa: a consequence of subduction-driven overthickening and collapse of mid-Archean continental crust. In: Benn, K., Mareschal, J.-C., Condie, K. (Eds.), Archean Geodynamics and Environments. American Geophysical Union Geophysical Monograph Series. Vol. 164, pp. 239–254.
Diener, J.F.A., Stevens, G., Kisters, A.F.M., Poujol, M., 2005. Metamorphism and exhumation of the basal parts of the Barberton greenstone belt, South Africa: constraining the rates of Mesoarchean tectonism. Precambrian Res. 143, 87–112.
Dixon, J.M., Summers, J.M., 1983. Patterns of total and incremental strain in subsiding troughs – experimental centrifuged models of inter-diapir synclines. Can. J. Earth Sci. 20, 1843–1861.

Dziggel, A., Armstrong, R.A., Stevens, G., Nasdala, L., 2005. Growth of zircon and titanite during metamorphism in the granitoid-gneiss terrane south of the Barberton greenstone belt, South Africa. Mineral. Mag. 69, 1019–1036.
Fischer, R., Gerya, T., 2016a. Regimes of subduction and lithospheric dynamics in the Precambrian: 3D thermomechanical modeling. Gondwana Res. 37, 53–70.
Fischer, R., Gerya, T., 2016b. Early earth plume-lid tectonics: a high-resolution 3D numerical modelling approach. J. Geodyn. 100, 198–214.
François, C., Philippot, P., Rey, P., Rubatto, D., 2014. Burial and exhumation during Archean sagduction in the east Pilbara Granite-Greenstone Terrane. Earth Planet. Sci. Lett. 396, 235–251.
Gardiner, N.J., Hickman, A.H., Kirkland, C.L., Lu, Y.-J., Johnson, T., Zhao, J.-X., 2017. Processes of crust formation in the early earth imaged through Hf isotopes from the East Pilbara Terrane. Precambrian Res. (in press).
Gerya, T.V., 2014. Precambrian geodynamics: concepts and models. Gondwana Res. 25, 442–463.
Gerya, T.V., Yuen, D.A., 2003a. Characteristics-based marker-in-cell method with conservative finite-differences schemes for modelling geological flows with strongly variable transport properties. Phys. Earth Planet. Inter. 140, 295–318.
Gerya, T.V., Yuen, D.A., 2003b. Rayleigh-Taylor instabilities from hydration and melt-ing propel “cold plumes” at subduction zones. Earth Planet. Sci. Lett. 212, 47–62.
Goscombe, B., Blewett, R.S., Czarnota, K., Groenewald, P.B., Maas, R., 2009. Metamorphic evolution and integrated terrane analysis of the Eastern Yilgarn Craton: rationale, methods, outcomes and interpretation. Geoscience Australia, Record 2009/23, p. 270.
Griffin, W.L., McGregor, V.R., Nutman, A., Taylor, P.N., Bridgwater, D., 1980. Early Archean granulite-facies metamorphism south of Ameralik, West Greenland. Earth Planet. Sci. Lett. 50, 59–74.
Grosch, E.G., Vidal, O., Abu-Alam, T., Mcloughlin, N., 2012. *P–T* constraints on the metamorphic evolution of the Paleoarchean Kromberg type-section, Barberton Greenstone Belt, South Africa. J. Petrol. 53, 513–545.
Herzberg, C., Asimow, P.D., Arndt, N., Niu, Y., Lesher, C.M., Fitton, J.G., Cheadle, M.J., Saunders, A.D., 2007. Temperatures in ambient mantle and plumes: constraints from basalts, picrites and komatiites. Geochem. Geophys. Geosyst. 8. http://dx.doi.org/10.1029/2006GC001390 (Q02006).
Herzberg, C., Condie, K., Korenaga, J., 2010. Thermal history of the earth and its petrological expression. Earth Planet. Sci. Lett. 292, 79–88.
Hickman, A.H., 1984. Archaean diapirism in the Pilbara Block, Western Australia. In: Kröner, A., Greiling, R. (Eds.), Precambrian Tectonics Illustrated. E. Schweizerbarts'che Verlagsbuchhandlung, Stuttgart, pp. 113–127.
Hickman, A.H., 2004. Two contrasting granite–greenstone terranes in the Pilbara Craton, Australia: evidence for vertical and horizontal tectonic regimes prior to 2900 Ma. Precambrian Res. 131, 153–172.
Hickman, A.H., Van Kranendonk, M.J., 2004. Diapiric processes in the formation of Archaean continental crust, East Pilbara Granite-Greenstone Terrane, Australia. In: Eriksson, P.G., Altermann, W., Nelson, D.R., Mueller, W.U., Catuneau, O. (Eds.), The Precambrian Earth: Tempos and Events. 54–75. Elsevier.
Johnson, T.E., Brown, M., Gardiner, N.J., Kirkland, C.L., Smithies, R.H., 2017. Earth's first stable continents did not form by subduction. Nature 543, 239–243.
Johnson, T.E., Brown, M., Goodenough, K.M., Clark, C., Kinny, P.D., White, R.W., 2016. Subduction or sagduction? Ambiguity in constraining the origin of ultramafic–mafic bodies in the Archean crust of NW Scotland. Precambrian Res. 283, 89–105.
Johnson, T.E., Brown, M., Kaus, B., Van Tongeren, J.A., 2014. Delamination and recycling of Archaean crust caused by gravitational instabilities. Nat. Geosci. 7, 47–52.
Johnson, T.E., Fischer, S., White, R., Brown, M., Rollinson, H., 2012. Archaean intracrustal differentiation from partial melting of metagabbro - field and geochemical evidence from the central region of the Neoarchaean Lewisian Complex, NW Scotland. J. Petrol. 53, 2115–2138.
Johnson, T.E., White, R.W., 2011. Phase equilibrium constraints on conditions of granulite-facies metamorphism at Scourie, NW Scotland. J. Geol. Soc. Lond. 168, 147–158.
Kamo, S.L., Davis, D.W., 1994. Reassessment of Archean crustal development in the Barberton Mountain Land, South Africa, based on U-Pb dating. Tectonics 13, 167–192.
Kisters, A.F.M., Anhaeusser, C.R., 1995. Emplacement features of Archaean TTG plutons along the southern margin of the Barberton greenstone belt, South Africa. Precambrian Res. 75, 1–15.
Kisters, A.F.M., Belcher, R.W., Poujol, M., Dziggel, A., 2010. Continental growth and convergence related arc plutonism in the Mesoarchaean: evidence from the Barberton granitoid greenstone terrain, South Africa. Precambrian Res. 178, 15–26.
Kisters, A.F.M., Stevens, G., Dziggel, A., Armstrong, R.A., 2003. Extensional detachment faulting and core complex formation in the southern Barberton granite-greenstone terrain, South Africa: evidence for a 3.2 Ga orogenic collapse. Precambrian Res. 127, 355–378.
Kitajima, K., Maruyama, S., Utsunomiya, S., Liou, J.G., 2001. Seafloor hydrothermal alteration at an Archaean mid-ocean ridge. J. Metamorph. Geol. 19, 583–599.
Kloppenburg, A., 2003. Structural evolution of the marble bar domain, Pilbara granite-greenstone terrain, Australia: the role of Archaean mid-crustal detachments. Geologica Ultraiectina, Mededelingen van de Faculteit Aardwetenschappen Universiteit Utrecht. 237 (257 p).
Kloppenburg, A., White, S.H., Zegers, T.E., 2001. Structural evolution of the Warrawoona Greenstone Belt and adjoining granitoid complexes, Pilbara Craton, Australia: implications for Archaean tectonic processes. Precambrian Res. 112, 107–147.
Korenaga, J., 2013. Initiation and evolution of plate tectonics on earth: theories and observations. Annu. Rev. Earth Planet. Sci. 41, 117–151.
Labrosse, S., Jaupart, C., 2007. Thermal evolution of the earth: secular changes and fluctuations of plate characteristics. Earth Planet. Sci. Lett. 260, 465–481.
Moore, W.B., Webb, A.A.G., 2013. Heat-pipe earth. Nature 501, 501–505.
Moyen, J.-F., Stevens, G., Kisters, A.F.M., 2006. Record of mid-Archean subduction from metamorphism in the Barberton terrain, South Africa. Nature 442, 559–562.
Moyen, J.-F., Van Hunen, J., 2012. Short-term episodicity of Archaean plate tectonics. Geology 40 (5), 451–454.
Nédélec, A., Chevrel, M.O., Moyen, J.F., Ganne, J., Fabre, S., 2012. TTGs in the making: natural evidence from Inyoni shear zone (Barberton, South Africa). Lithos 153, 25–38.
Nutman, A.P., McGregor, V.R., Shiraishi, K., Friend, C.R.L., Bennett, V.C., Kinny, P.D., 2002. >3850 Ma BIF and mafic inclusions in the early Archaean Itsaq Gneiss Complex around Akilia, southern West Greenland? The difficulties of precise dating of zircon-free protoliths in migmatites. Precambrian Res. 117, 185–224.
Percival, J.A., Skulski, T., Sanborn-Barrie, M., Stott, G.M., Leclair, A.D., Corkery, M.T., Boily, M., 2012. Geology and tectonic evolution of the Superior Province, Canada. In: Percival, J., Clowes, R., Cook, F.A. (Eds.), Tectonic Styles in Canada: The Lithoprobe Perspective. Geological Association of Canada, St. Johns, NL, Canada, pp. 321–378.
Powell, R., Holland, T.J.B., 2008. On thermobarometry. J. Metamorph. Geol. 26, 155–179.
Rozel, A.B., Golabek, G.J., Jain, C., Tackley, P.J., Gerya, T., 2017. Continental crust formation on early earth controlled by intrusive magmatism. Nature http://dx.doi.org/10.1038/nature22042.
Schoene, B., de Wit, M.J., Bowring, S.A., 2008. Mesoarchean assembly and stabilization of the eastern Kaapvaal craton: a structural-thermochronological perspective. Tectonics 27, TC5010. http://dx.doi.org/10.1029/2008TC002267.
Silver, P.G., Behn, M.D., 2008. Intermittent plate tectonics? Science 319, 85–88.
Sizova, E., Gerya, T., Brown, M., 2014. Contrasting styles of Phanerozoic and Precambrian continental collision. Gondwana Res. 25, 522–545.
Sizova, E., Gerya, T., Brown, M., Perchuk, L., 2010. Subduction styles in the Precambrian: insight from numerical experiments. Lithos 116, 209–229.
Sizova, E., Gerya, T., Stüwe, K., Brown, M., 2015. Generation of felsic crust in the Archean: a geodynamic modeling perspective. Precambrian Res. 271, 198–224.
Syracuse, E.M., van Keken, P.E., Abers, G.A., 2010. The global range of subduction zone thermal models. Phys. Earth Planet. Inter. 183, 73–90.
Terabayashi, M., Masadab, Y., Ozawa, H., 2003. Archean ocean-floor metamorphism in the North Pole area, Pilbara Craton, Western Australia. Precambrian Res. 127, 167–180.
Thébaud, N., Rey, P.F., 2013. Archean gravity-driven tectonics on hot and flooded continents: controls on long-lived mineralized hydrothermal systems away from continental margins. Precambrian Res. 229, 93–104.
Van Hunen, J., Moyen, J.-F., 2012. Archean subduction: fact or fiction? Annu. Rev. Earth Planet. Sci. 40, 195–219.
Van Kranendonk, M.J., 2010. Two types of Archean continental crust: plume and plate tectonics on early earth. Am. J. Sci. 310, 1187–1209.
Van Kranendonk, M.J., 2011. Cool greenstone drips and the role of partial convective overturn in Barberton greenstone belt evolution. J. Afr. Earth Sci. 60, 346–352.
Van Kranendonk, M.J., Collins, W.J., Hickman, A.H., Pawley, M.J., 2004. Critical tests of vertical vs horizontal tectonic models for the Archaean east Pilbara granite-greenstone Terrane, Pilbara Craton, Western Australia. Precambrian Res. 131, 173–211.
Van Kranendonk, M.J., Kröner, A., Hegner, E., Connelly, J., 2009. Age, lithology and structural evolution of the c. 3.53 Ga Theespruit formation in the Tjakastad area, southwestern Barberton Greenstone belt, South Africa, with implications for Archean tectonics. Chem. Geol. 261, 114–138.
Van Kranendonk, M.J., Kröner, A., Hoffman, E.J., Nagel, T., Anhaeusser, C.R., 2014. Just another drip: re-analysis of a proposed Mesoarchean suture from the Barberton Mountain Land, South Africa. Precambrian Res. 254, 19–35.
Van Kranendonk, M.J., Smithies, R.H., Griffin, W.L., Huston, D.L., Hickman, A.H., Champion, D.C., Anhaeusser, C.R., Pirajno, F., 2014. A volcanic plateau origin for Paleoarchean lithosphere of the Pilbara and Kaapvaal cratons. In: Roberts, N.M., van Kranendonk, M., Parman, S., Shirey, S., Clift, P.D. (Eds.), Continental Growth Through Time. 389. Geological Society, London, Special Publications, pp. 83–111.
Van Kranendonk, M.J., Smithies, R.H., Hickman, A.H., Champion, D.H., 2007. Secular tectonic evolution of Archaean continental crust: interplay between horizontal and vertical processes in the formation of the Pilbara Craton, Australia. Terra Nova 19, 1–38.
Van Thienen, P., Van den Berg, A.P., 2004. On the formation of continental silisic melts in thermochemical mantle convection models: implication for early earth. Tectonophysics 394, 111–124.
Vogt, K., Gerya, T., Castro, A., 2012. Crustal growth at active continental margins: numerical modeling. Phys. Earth Planet. Inter. 192–193, 1–20.
Wiemer, D., Schrank, C.E., Murphy, D.T., Hickman, A.H., 2016. Lithostratigraphy and structure of the early Archaean Doolena gap greenstone belt, east Pilbara Terrane, Western Australia. Precambrian Res. 282, 121–138.
Williams, I.S., Collins, W.J., 1990. Granite-greenstone terranes in the Pilbara Block, Australia, as coeval volcano-plutonic complexes; evidence from U-Pb zircon dating of the Mount Edgar Batholith. Earth Planet. Sci. Lett. 97, 41–53.
Windley, B.F., Bridgwater, D., 1971. The evolution of Archaean low- and high-grade terrains. 3. Geological Society of Australia, Special Publication, pp. 33–46.